Results in Physics 15 (2019) 102584

Contents lists available at ScienceDirect

Results in Physics

journal homepage: www.elsevier.com/locate/rinp

Fabrication of energy storage EDLC device based on CS:PEO polymer blend electrolytes with high Li^+ ion transference number

Shujahadeen B. Aziz[a,b,*], M.H. Hamsan[c], M.A. Brza[d], M.F.Z. Kadir[c], Rebar T. Abdulwahid[e], Hewa O. Ghareeb[f], H.J. Woo[g]

[a] Advanced Polymeric Materials Research Lab., Department of Physics, College of Science, University of Sulaimani, Qlyasan Street, Sulaimani, Kurdistan Regional Government, Iraq
[b] Komar Research Center (KRC), Komar University of Science and Technology, Kurdistan Regional Government, Sulaimani 46001, Iraq
[c] Centre for Foundation Studies in Science, University of Malaya, Kuala Lumpur, Malaysia
[d] Faculty of Engineering, International Islamic University of Malaysia, Kuala Lumpur, Gombak, Malaysia
[e] Department of Physics, College of Education, University of Sulaimani, Kurdistan Regional Government, Old Campus, Sulaimani, Iraq
[f] Department of Chemistry, College of Science, University of Sulaimani, Kurdistan Regional Government, Qlyasan Street, Sulaimani, Iraq
[g] Centre for Ionics, Faculty of Science, University of Malaya, Kuala Lumpur, Malaysia

ARTICLE INFO

Keywords:
Polymer blend electrolytes
XRD and FTIR study
TNM and LSV analysis
Cyclic voltammetry
EDLC

ABSTRACT

High ion transference number polymer blend electrolytes of chitosan (CS):poly (ethylene oxide) (PEO):$LiClO_4$ systems were synthesized using solution cast technique. The XRD analysis indicated that the crystalline peaks of CS vanished in CS:PEO host blend polymer. The intensity of the hump observed in CS:PEO blend film decreased upon addition of $LiClO_4$ salt. The FTIR study revealed the complex formation between the CS:PEO and added salt through the shifting and lessening in intensity of the FTIR bands corresponding to the functional groups. The bulk resistance estimated from the impedance plots decreased with increasing salt concentration. The maximum DC conductivity was found to be 7.34×10^{-4} S cm^{-1} for CS:PEO incorporated with 40 wt% of $LiCLO_4$ salt. The electrical equivalent circuit (EEC) model has been carried out for selected samples to clarify the common picture of the electrical properties of the system. It has been verified via transference number analysis (TNM) that the transport mechanism in CS:PEO:$LiClO_4$ electrolyte is predominantly ionic in nature with $t_{ion} = 0.993$ and $t_{el} = 0.007$. The high ion transference number and high DC conductivity emphasized the possibility of the samples for electrochemical device application. From linear sweep voltammetry (LSV) investigation, CS:PEO:$LiClO_4$ electrolyte was found to be electrochemically constant as the voltage sweep linearly up to 2.24 V. The CV curve covered most of the area of the current–potential plot with no redox peaks. The DC conductivity value, TNM and LSV results revealed the availability of the samples for electrical double layer capacitor (EDLC) application. The existence of charges double-layer in the fabricated EDLC was proven from cyclic voltammetry (CV). EDLC showed a consistent performance of specific capacitance (6.88 F g^{-1}), energy density (0.94 Wh kg^{-1}) and power density (305 W kg^{-1}) for complete 100 cycles at a current density of 0.5 mA cm^{-2}.

Introduction

A series of research initiatives have focused on amorphous polymer salt complexes with respect to the promising role they could play in various devices, including fuel cells, batteries, electrochromic displays, sensors, and supercapacitors [1–3]. Applications in these areas have been identified as viable because the polymer electrolytes are associated with numerous advantages in comparison to traditional materials. As documented in the literature, these advantages range from straightforward processing, cost-effectiveness, and productivity to the lack of internal shorting and leakage of electrolytes [4,5]. At the same time, in comparison with inorganic solids, polymer electrolytes are superior in terms of flexibility [6]. Polymer electrolytes can be prepared by dissolving metal salts in a polymeric matrix and consequently dissociated into metal cations and corresponding counter anions. These types of polymers are conductive ionically and thereby have received considerable attention owing to their applications in versatile electrochemical devices [7]. Natural polymers are also environmentally

* Corresponding author at: Advanced Polymeric Materials Research Lab., Department of Physics, College of Science, University of Sulaimani, Qlyasan Street, Sulaimani, Kurdistan Regional Government, Iraq.
E-mail addresses: shujahadeenaziz@gmail.com, shujaadeen78@yahoo.com, shujahadeen.aziz@univsul.edu.iq (S.B. Aziz).

https://doi.org/10.1016/j.rinp.2019.102584
Received 12 June 2019; Received in revised form 31 July 2019; Accepted 10 August 2019
Available online 19 August 2019

friendly solid polymer electrolytes and showed important characteristics to be implemented in electrochemical devices such as electrochromic devices, high energy density batteries, sensors and fuel cells [8]. Solid polymer electrolytes are interesting alternative to liquid electrolytes in dye-sensitized solar cells [9–13]. Recently, biodegradable nature of natural polymers, for example, starch, cellulose, chitosan, carrageenan, and agarose have shown promising characteristics to be intensively explored by many researcher groups as those are non-toxic and easy to use in electrolyte preparation [14]. For example, Chitosan (CS) as deacetylated product is one derivatives of chitin, together with cellulose are one of the most abundant biopolymer in nature [15]. It is mainly obtained from shrimp waste and considerably used as a natural polymer in many potential applications [16]. The best available knowledge indicates that as a result of the enrichment in polar groups (NH_2 and OH) within the chains and served as conjunction sites, chitosan is a prevalent sorbent with a high affinity for transition metal ions [17]. The capacity that the chitosan has for moulding into a range of forms is considered as a vital property, with these forms ranging from hydrogels and porous scaffolds to films [18]. Several ion-conducting polymer electrolytes based on chitosan have been documented, including CS-NH_4NO_3-EC [19], CS- $NH_4CF_3SO_3$ [20], CS -$LiCF_3SO_3$-EC [21], CS -NH_4I-EC [22], CS -PVA-NH_4NO_3-EC [23], CS -NaClO4 [24] and CS -$AgNO_3$ [25]. The most obvious properties of chitosan are relatively crystalline in structure, high molecular weight polysaccharide and robust structure as a result of intermolecular or intramolecular hydrogen bonds [26,27]. The applicability of chitosan depends on increasing both amorphous phase and ionic conductivity in polymers; additionally, blending of polar polymer methodology has been reported [28,29].

In the present work, chitosan is combined with PEO polymer. Several polymers, including polyvinyl pyrrolidone (PVP) [28], boroxine ring polymer (BP) [29], polyacrylonitrile (PAN) [30,31], and poly(dithiooxamide) (PDTOA) [32] have been mixed with PEO based electrolytes. Based on previous work [33], the optimum ratio is 70 wt% chitosan and 30 wt% PEO where amorphous structure was prevalent. Similarly, in the present work, 70 wt% chitosan- 30 wt% PEO is chosen with various concentration of lithium perchlorate ($LiClO_4$). Thereby, a relatively highest conducting electrolyte has been obtained as electrode separators in the EDLC. EDLC is considered as an alternative for conventional batteries. The mechanism of energy storage for EDLC involves non-Faradaic process where there is no electron exchange and alternatively ions establish double-layer on the carbon-based electrodes [34]. Advantages involving EDLC are relatively higher power density, durable, better thermal stability, higher reversibility, cheaper, safer and simpler fabrication methods when compared to Faradaic capacitor or pseudocapacitor [35-37]. Therefore, the main aim of the current work is to investigate the suitability of CS:PEO based polymer electrolyte for EDLC applications.

Experimental method

Materials and sample preparation

High molecular weight chitosan (CS) (average molecular weight 310,000–375,000) and poly (ethylene oxide) powder (average molecular weight 300,000) materials were supplied by Sigma-Aldrich. For the preparation of the polymer blend based on chitosan: poly(ethylene oxide) [CS:PEO], 70 wt% chitosan and 30 wt% poly(ethylene oxide) were dissolved separately, each in 50 mL of 1% acetic acid at room temperature for 120 min. Subsequently, the solution mixed and stirred for 3 h to obtain a homogeneous blending solution. For the blended solution of CS:PEO, different amounts of $LiClO_4$ from 10 to 40 wt% in steps of 10 were added separately with continuous stirring to obtain CS: PEO: $LiClO_4$ electrolytes. The polymer blend electrolytes were coded as CSPB1, CSPB2, CSPB3, and CSPB4 for CS: PEO incorporated with 10, 20, 30, and 40 wt% of $LiClO_4$, respectively. Following casting in the labelled Petri dishes, films were formed by leaving the solutions to dry at room temperature and the resulting films were further dried in a desiccator. In this way, the procedure allowed generating the films containing no solvents, and the fabricated polymers have been utilized as raw materials.

TNM and LSV measurements

V & A Instrument DP3003 digital DC power supply was employed to perform the transference number (TNM) analysis via DC polarization method [38]. The highest conducting electrolyte was sandwiched between blocking electrodes (stainless steel) of a Teflon holder. The cell was polarized at 30 mV and the DC current monitored as a function of time at the ambient temperature. The potential stability of the electrolyte was explored using linear sweep voltammetry (LSV) analysis (DY2300 potentiostat). The relatively high conducting electrolyte was placed between two stainless steel in Teflon conductivity holder at a scan rate used was 50 mV s^{-1}.

EDLC preparation

A 0.50 g of polyvinylidene fluoride (PVdF) was stirred in 15 mL N-methyl pyrrolidone (NMP). Activated carbon (3.25 g) and carbon black (0.25 g) powders were mixed using planetary ball miller to gain a homogeneous solution. The mixture of activated carbon and carbon black was poured in the PVdF solution. The homogeneous solution was doctor bladed on aluminum foil and heated at 60 °C for a certain time. The electrodes were stored in a dessicator filled with silica gel. The relatively high conducting electrodes was sandwiched between two carbon electrodes and packed in CR2032 coin cells. The galvanostatic charge-discharging characteristics of the EDLC were performed using a battery cycler (Neware) with a current density of 0.5 mA cm^{-2}. Digi-IVY DY2300 Potentiostat was used to carry out cyclic voltammetry (CV) of the EDLC in the potential window of 0 to 1 V at 10 mV s^{-1}. The schematic diagram of the EDLC cell was shown in scheme 1.

Structural and impedance characterizations

Spotlight 400 Perkin-Elmer spectrometer was used to conduct Fourier transform Infrared (FTIR) spectroscopy with a resolution of 1 cm^{-1} (450–4000 cm^{-1}). The XRD analysis was performed via D5000 X-ray diffractometer (1.5406 Å). The 2θ angle was varied from 5° to 80° (Resolution = 0.1°). The HIOKI 3532–50 LCR HiTESTER, which hyphenates to a computer in the 42 Hz to 5,000 kHz frequency range, was employed to measure the films' impedance at the room temperature. The usage of the software is to control the measurements as well as the calculation of both the imaginary and real parts of the impedance spectrum. Discs with a diameter of 20 mm were produced from the SPE

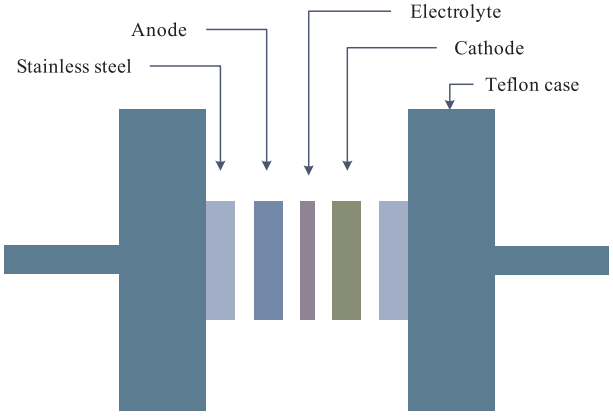

Scheme1. Diagram of the EDLC cell.

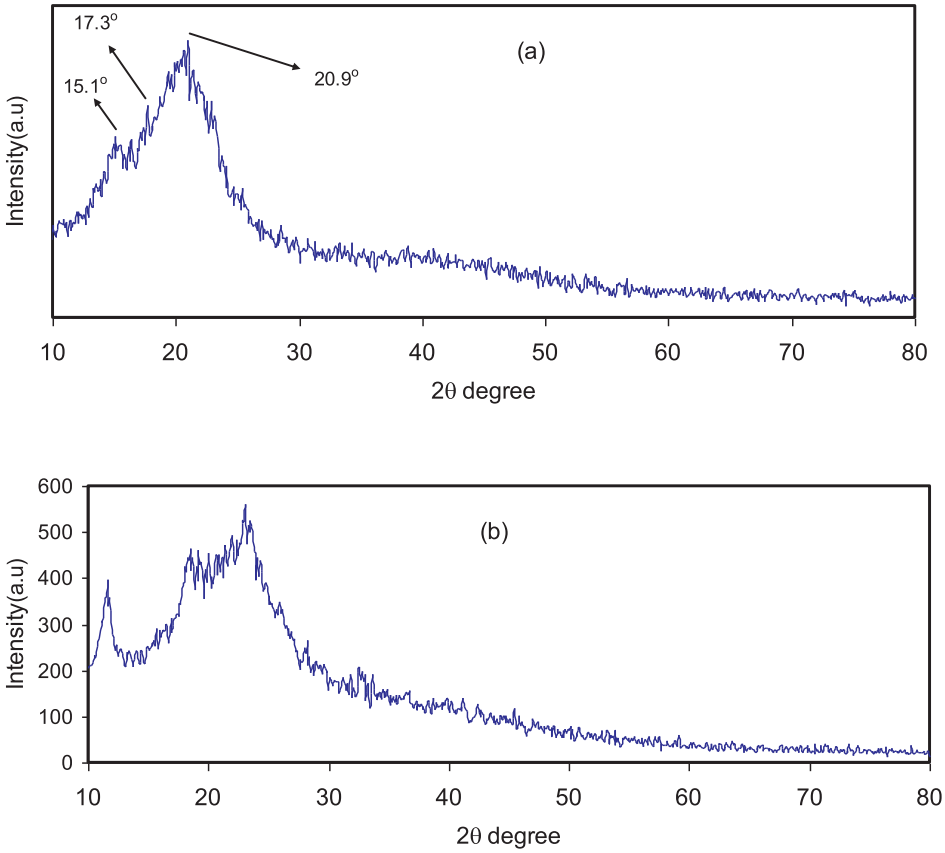

Fig. 1. XRD pattern for (a) pure CS and (b) CS:PEO films.

films and, in turn, these were sandwiched within a pair of stainless steel electrodes under spring pressure. For the complex impedance (Z*), the imaginary (Z_i) and real (Z_r) parts were employed using the relations given below to calculate the dc conductivity (σ_{dc}).

$$\sigma_{dc} = \left(\frac{1}{R_b}\right) \times \left(\frac{t}{A}\right) \quad (1)$$

where t is the thickness and A is the area of the film, R_b is the bulk resistance of the film derived from the intercept of the impedance plot on the real axis.

Results and discussion

XRD study

To investigate the structural behavior of the samples, the XRD patterns were acquired. The XRD patterns of pure CS and CS: PEO films are shown in Fig. 1(a,b). Evidence revealed that pure chitosan is characterised by a semi-crystalline structure. From Fig. 1a, it can be clearly noted that CS possess a range of crystalline peaks. Regarding pure chitosan's XRD pattern, two characteristic peaks at near 2θ° = 15° and 20° demonstrate the crystalline part of the pure chitosan membrane's average intermolecular distance [39,40]. Chitosan's rigid crystalline structure is primarily kept through hydrogen bonding (both intermolecular and intramolecular), which is the product of amino and hydroxyl groups by means of an absorbed water molecule [41,42]. The intermolecular hydrogen bonds can easily be disrupted as a result of blending of PEO with CS polymer. There is a clear lessening in the crystalline peaks of pure CS compared to CS: PEO blend film. The XRD pattern for the selected samples of the blend electrolytes incorporated with $LiCLO_4$ are shown in Fig. 2(a,b). It can be observed (see Fig. 2a) that with addition of 20 wt% of $LiClO_4$ salt, the crystalline peaks in CS:PEO are almost disappeared and the intensity of the peak moderately decreased. Nevertheless, with the addition of 40 wt% of $LiClO_4$ (see Fig. 2b), CS: PEO's hump exhibited broad, and more lesser in the intensity of the peak. This is due to the elimination of the hydrogen bonding between amino groups and hydroxyl groups, which is responsible for complexation between lithium perchlorate salt and CS:PEO. Hence, the amorphous phase predominates within the sample, and a few crystalline peaks with low intensities are exist [43,44]. The new peaks can be ascribed to a sort of short-range order, which is established as a result of ion multiples existence [45]. It is interesting to note, though, Sanders et. al [46] have accounted for the new peaks with reference to the complex development between polymer and salt as opposed to pure salt.

FTIR analysis

Fourier transform infrared (FTIR) spectroscopy has been widely used in the study of the formation of polymeric blends. FTIR spectroscopy provides information regarding functional groups as well as the intermolecular interaction via analysis of FTIR spectra corresponding to stretching or bending vibrations of particular bonds [47]. FTIR was carried out in order to determine the shifting and variation in intensity of the bands due to functional groups in pure CS: PEO and CS: PEO: $LiClO_4$ electrolyte samples. The literature reported that a key variable when determining a desired polymer host is the availability of heteroatoms (e.g., O and N) that contain lone pair electrons [18]. Moreover, it was reported in literature [5], that chain polymers in which the electro-negative atoms (i.e., oxygen or nitrogen) are present in their repeating units can act as solvents for a certain salt, which is attributable to the complexation between cations and electro-negative atoms. Moreover, studies have indicated that CS polymer is identified by a lone amino group and a pair of hydroxyl groups in its repeat unit [48,49].

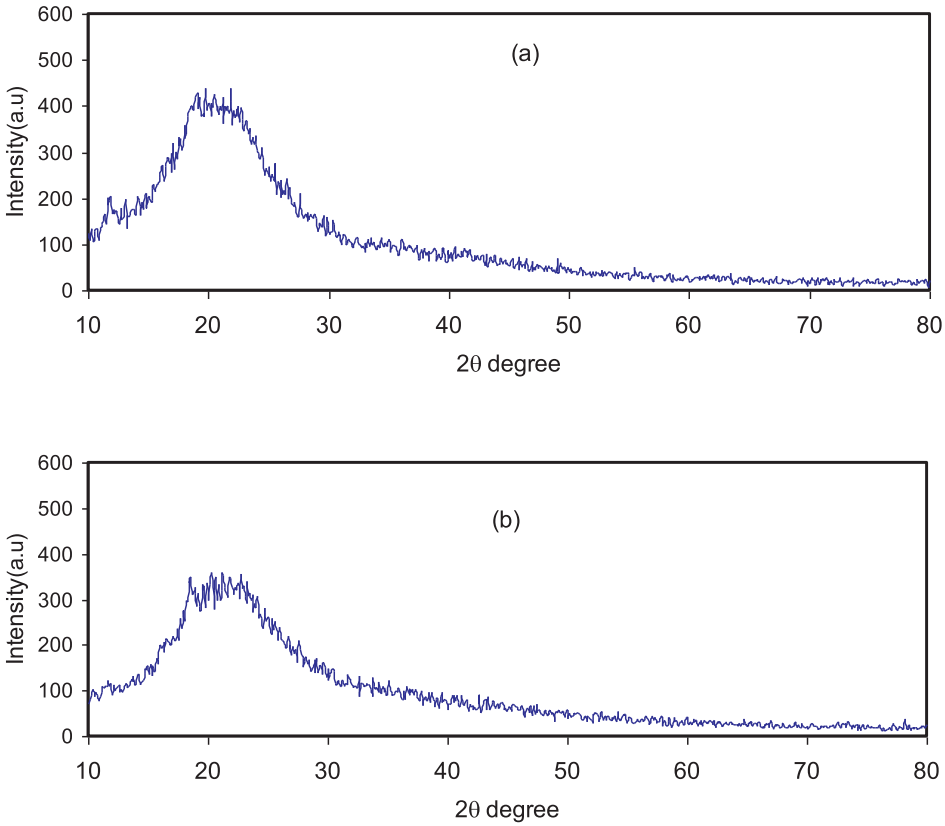

Fig. 2. XRD pattern for (a) CSPB2 and (b) CSPB4 blend electrolyte films.

Fig. 3(a,b) shows the FTIR spectra for pure CS:PEO and CS:PEO:$LiClO_4$ complexes at various regions of infrared radiations. In the previous work [50], it was observed that the broad peak at around 3559 cm^{-1} associated with the −OH stretching and the strong peak at around 2900 cm^{-1} ascribed to the C−H stretching modes of PEO which are deeply affected by doping materials. In Fig. 3b, it is interesting to look at the peak resulted from C-H stretching (2904 cm^{-1}) broadening with increasing $LiClO_4$ to CS: PEO and almost disappeared at 40 wt% of $LiClO_4$ salt. The shift and reduction in intensity are indicators for the complex development between the dopant salt and CS:PEO. Each sample is linked with the primary absorption peaks features, containing vibration of amino group (NH_2), O═C−NHR, and hydroxyl (OH) functional groups of CS. In view of Fig. 3a, it is apparent that there are shifts to lower wave numbers in the amine (NH_2), O═C−NHR and (OH) groups bands, which is inductor for the complexation between the $LiClO_4$ salt and CS: PEO [51,52]. Regarding the relative intensity of the bands, the lessening, broadening, and shifting in intensity are indicative for the electrostatic interaction between the functional groups of the CS: PEO polymer blenders and the ions [53]. Moreover, the shift of vibrational bands in the direction of lower wave numbers is indicative of the increasingly weak nature of the intermolecular and intramolecular hydrogen bonds that exist between polymer chains [49], and thus an increase of amorphous phases.

Impedance analysis

The AC conductivity principle's complex impedance spectroscopy measurements rely on assessments of cell impedance/admittance over multiple frequencies, as well as the analysis of these in complex impedance planes. As a comparatively thorough concept when considered in relation to resistance, impedance is marked by the way in which it accounts for phase difference. In AC, the impedance (Z) is employed as opposed to the resistance, which can be computed by adding the resistance to the reactance [54]. Fig. 4(a–e) illustrates the electrical impedance plots (Z_i vs Z_r) for CS:PEO and CS:PEO:$LiClO_4$ complexes. Clearly, with increasing salt concentration the bulk resistance (see the insets) decreased. A noteworthy feature of the Figures is that a pair of distinct regions predominates. First, a high frequency semicircle region arises from the solid electrolyte's bulk effect; next a low frequency spike region arises due to electrode polarization (EP) (that is, the effect of blocking electrodes). EP occurs as a result of the emergence of electric double layer (EDL) capacitances, which themselves arise from free charge accumulation at the solid electrolyte and electrode surface interfaces [55]. Here, it is necessary for the complex impedance plots at a low frequency region to display a straight line parallel to the imaginary axis. In other words, while the straight line's inclination ought to be 90°, the blocking double-layer capacitance (EP phenomena) at the blocking electrodes brings about the inclination [56,57]. Table 1 lists the DC conductivity of pure CS:PEO and CS:PEO:$LiClO_4$ electrolyte samples at ambient temperature. It is interesting to note that the DC conductivity increased from 7.16×10^{-10} S cm^{-1} for pure CS:PEO to 7.34×10^{-4} S cm^{-1} for CS:PEO incorporated with 40 wt% of $LiClO_4$. The low DC conductivity (high resistance, $4x10^6$ Ohm) of pure CS:PEO reveals the insulating properties of polymers without dopant charge carriers. Previous studies confirmed that polymer electrolytes with high DC conductivity ranging from 10^{-5} to 10^{-3} S cm^{-1} are crucial for electrochemical device applications including batteries and electrical double layer capacitors (EDLCs) [23,24,38].

Commonly, modeling and analysis of the spectra of impedance are eased with an equivalent circuit, which stemmed from the fact that it is a straightforward and offers the mechanism of the system [58]. Fig. 5(a,b) displays the experimental impedance plots with electrical equivalent circuits (EEC) for chosen samples. The EEC model is fundamental to comprehend the electrical properties of polymer based solid electrolytes. It is possible to represent experimental impedance plots using a three-component equivalent circuit. More specifically, the

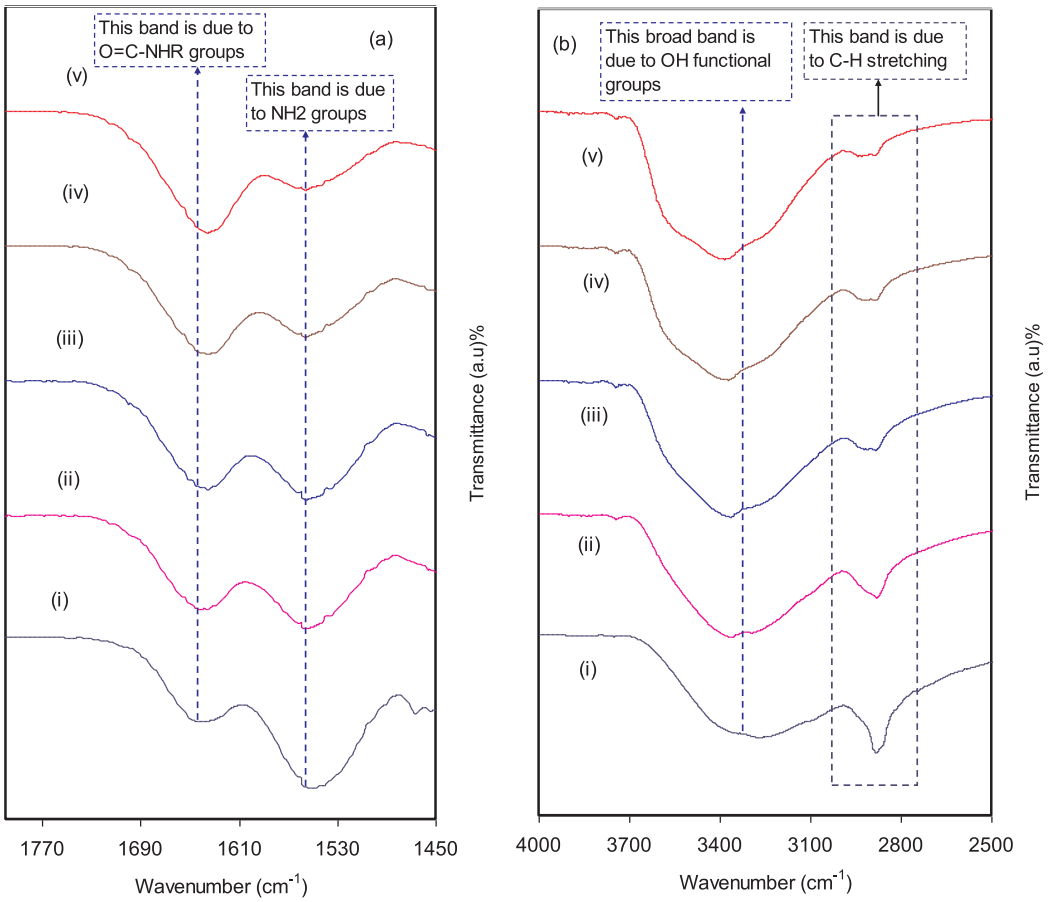

Fig. 3. FTIR spectra of (i) CS:PEO (pure film), (ii) CSPB1, (iii) CSPB2, (iv) CSPB3, and (v) CSPB4 in the region (a) 1450 cm^{-1} to 1800 cm^{-1}, and (b) 2500 cm^{-1} to 4000 cm^{-1}.

three principal components are ZCPE1, a constant phase element; ZCPE2, another constant phase element; and a bulk resistance (R_b) for the solid polymer electrolyte (see inset of Fig. 5a). R_b and ZCPE1 are reflected in the high frequency region, whilst the low frequency spike region is connected to ZCPE2. This is indicative to the double layer capacitance appearing at the interface between the electrodes and the solid polymer electrolyte [59]. It is possible to derive ZCPE's impedance as [60-62]:

$$Z_{CPE} = \frac{\cos(\pi n/2)}{Y_m \omega^n} - j\frac{\sin(\pi n/2)}{Y_m \omega^n} \tag{2}$$

where Y_m refers to the CPE capacitance, ω is the angular frequency and n is correlated to the deviation of the plot from the vertical axis in complex impedance plots. In particular, CPE is acronym commonly applied instead of capacitor in the context of a modeled equivalent circuit. The reason behind this is the behavior of solid polymer electrolytes differing from the behavior of an ideal or pure capacitor. This implies an ideal semi-circular pattern [59], which it is not possible to identify in existing experimental impedance plots. In this case, it is possible to express the real (Z_r) and imaginary (Z_i) complex impedance (Z^*) values in the equivalent circuit (insets of Fig. 5(a,b)) in the following way:

$$Z_r = R_s + \frac{R_1 + R_1^2 Y_1 \omega^{n1} \cos(\pi n_1/2)}{1 + 2R_1 Y_1 \omega^{n_1} \cos(\pi n_1/2) + R_1^2 Y_1^2 \omega^{2n_1}} + \frac{\cos(\pi n_2/2)}{Y_2 \omega^{n_2}} \tag{3}$$

$$Z_i = \frac{R_1^2 Y_1 \omega^{n_1} \sin(\pi n_1/2)}{1 + 2R_1 Y_1 \omega^{n_1} \cos(\pi n_1/2) + R_1^2 Y_1^2 \omega^{2n_1}} + \frac{\sin(\pi n_2/2)}{Y_2 \omega^{n_2}} \tag{4}$$

It is obvious that the semicircle diameter shrunk at the high frequency region under a rising concentration of salt (20 wt% of $LiClO_4$). Fig. 5a shows that the incomplete semicircle corresponds to R_b in parallel with CPE element and in series with another CPE corresponding to low frequency tail (see the inset of Fig. 5a). Furthermore, at 30 wt% and 40 wt% of $LiClO_4$, the incomplete semicircle vanished completely (see Fig. 4(c-e), which indicates that it is feasible to consider merely the resistive behavior of the solid polymer electrolyte and the CPE component in series. A vital implication of the outcome is that the semicircle vanished at the high frequency region of the impedance plot. Hence, the entire conductivity can be attributed to transportation of ions [63]. In this case, the values of Z_r and Z_i associated to the EEC can be expressed as:

$$Z_r = R + \frac{\cos(\pi n/2)}{Y_m \omega^n} \tag{5}$$

$$Z_i = \frac{\sin(\pi n/2)}{Y_m \omega^n} \tag{6}$$

EDLC study

Increasing harmless electrolytes mainly solid polymer electrolytes (SPEs) is an essential part of research for the application of electrochemical devices. Even though this compound system being initiated since late seventieth, it still believed one of the leading subjects [64,65]. To use the polymer electrolyte for application it is essential to study the transference number analysis (TNM) and linear sweep voltammetry (LSV). In polymer electrolyte, it is crucial to determine the dominant charge carrier species, which can be done using TNM. The DC polarisation technique was employed to assess the sample's ionic

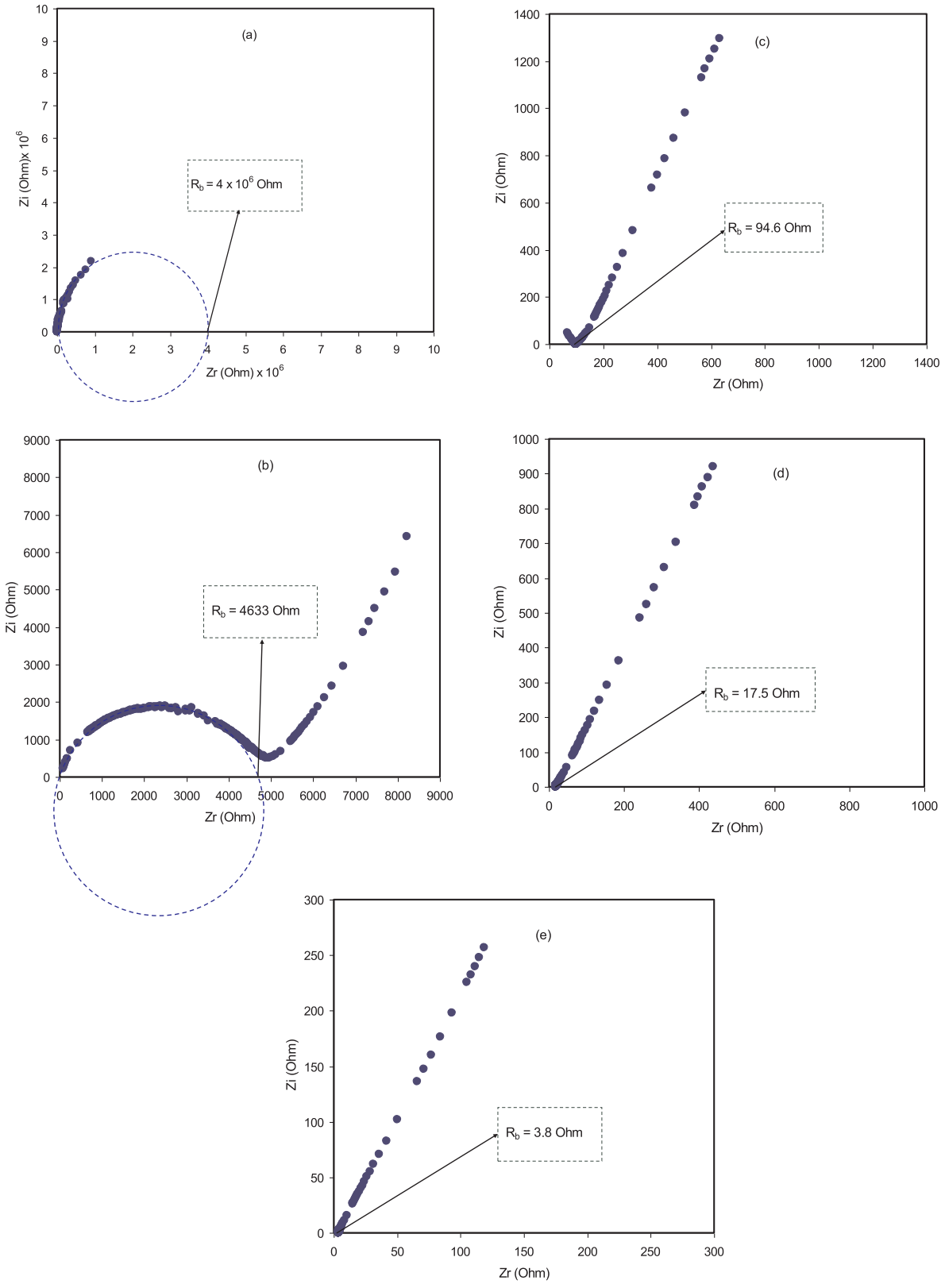

Fig. 4. Experimental Impedance plots for (a) pure CS:PEO film (b) CSPB1, (c) CSPB2, (d) CSPB3, and (e) CSPB4 blend electrolyte films.

transference number (t_{ion}). The technique involves the application of DC voltage to the sample underneath its decomposition potential, which is followed by the examination of the resulting currents in relation to time (see Fig. 6) [66]. The polymer electrolyte with the maximum conductivity was positioned between a pair of stainless steel blocking electrodes (SS) to ease the measurement, and it is likely to employ the following equation to estimate both the ion (t_{ion}) and the electron (t_{el}) transference number:

Table 1
DC conductivity for pure CS:PEO and blend electrolyte films at room temperature.

Sample Designation	DC conductivity (S cm^{-1})
CS:PEO	7.16×10^{-10}
CSPB1	6.18×10^{-7}
CSPB2	3.02×10^{-5}
CSPB3	1.63×10^{-4}
CSPB4	7.34×10^{-4}

$$t_{ion} = \frac{I_i - I_{ss}}{I_i} \tag{7}$$

$$t_{ion} = 1 - t_{el} \tag{8}$$

Here I_{ss} is the steady-state current and I_i is the initial current. The I_i is observed at 31μA. The large value of initial current is due to the contribution of both ion and electron at the initial stage. As the used electrodes are stainless steel which is known to block ions, thus a drastic drop of current is noticed before constant at 0.20 μA [67]. This phenomenon depicts the ionic conductor behavior [68]. Since $t_{ion} = 0.993$ and $t_{el} = 0.007$, the outcome demonstrates that the ions are the dominant charge carriers through the polymer electrolyte. The proximity of t_{ion} to 1, the ideal value, is a particularly noteworthy result, which indicates that the nature of the prepared electrolyte film's transport mechanism is primarily ionic [66,69].

Another vital parameter that can be evaluated for the application standpoint in electrochemical devices (e.g. supercapacitors) is the working voltage range, frequently referred to as electrochemical stability [70]. The study used LSV, facilitated by stainless steel electrodes, to test the electrochemical stability of every polymer electrolyte, and Fig. 7 presents a typical LSV plot for the highest conducting CS:PEO:-$LiClO_4$ blend electrolyte. The outcomes indicate that, from the EDLC application viewpoint [71], the electrochemical stability is in the satisfactory working voltage range of 2.24. Monisha et al. [72] reported that the threshold voltage is that the current passes through the cells. Shukur et al. [61] demonstrated a decomposition voltage of 2.10 V for lithium salt based biopolymer electrolyte. Thus, the potential stability, i.e potential window of the relatively high conducting electrolyte in this work is suitable for energy storage device applications.

Cyclic voltammetric tests can be used to grow insight into the nature of charge storage at the electrodes-electrolyte interfaces in the EDLC study. Moreover, it is likely to use the CV of EDLC cells to collect information about the charge storage nature at the single interfaces in the cathodic and anodic regions [73]. In Fig. 8, the room temperature CV of the assembled cell is presented, with a notable finding being the lack of a redox peak. This indicates that a non-Faradaic process has taken place in the current electrolyte system. Additionally, EDLC's charge storage mechanism relies on ion accumulation at the interfaces between electrodes and electrolytes in the context of electric potential application [74]. A noteworthy feature of Fig. 8, is that it is close to the ideal EDLC which has an exact rectangular shape. The leaf-shaped pattern of CV plot it means the system follows nearly rectangular shape [74,75]. Fast build-up of the electric double layer and internal resistance of EDLC are often cited as the reasons for non-rectangular shapes. In the case of internal resistance, this is reflected in a sudden voltage drop when discharging the EDLC, also known as Vdrop (see charge–discharge curve) [74,76,77]. Since the diagram of CV reveals no clear reversible humps, it is sensible to conclude that a fast Faradaic reversible reaction has not happened alongside the formation of the double layer [78].

The electrochemical capacitance of materials can also be evaluated by considering the cyclic discharge. Fig. 9 reveals the galvanostatic charge–discharge curves of the assembled EDLC cells at ambient temperature for CS: PEO incorporated with 40 wt% of $LiClO_4$. The discharge curves show that the EDLC cells display linear characteristics, indicative of excellent electrochemical performance from the EDLC [79]. Note worthily, the EDLC cells also display linear discharge behavior involving a small ohmic drop, thus suggesting a non-Faradic capacitive charge-storage mechanism [80]. Since the discharge curve's slope is presented as (x), the EDLC cells' C_{spe} can be determined using the following equation:

$$C_{spe} = \frac{i}{xm} \tag{9}$$

Here i is the applied current. Fig. 10 shows the C_{spe} versus cycle number. The capacitance value obtained from this current work is relatively higher than the previous literature. The maximum average C_{spe} is 6.88F g^{-1}. This capacitance synthesized in the present work is of the great interest compared to the specific capacitance values of 2.6–3.0 and 1.7–2.1 F g^{-1} which recorded for the EDLC cells with the Mg- and Li-based PEO polymer electrolytes incorporated with ionic liquids [73]. It is clear that the capacitance almost constant over 100 cycles. While in other reports huge reduction of C_{spe} was observed at large number of cycles. The researchers considered that ion aggregate formation could

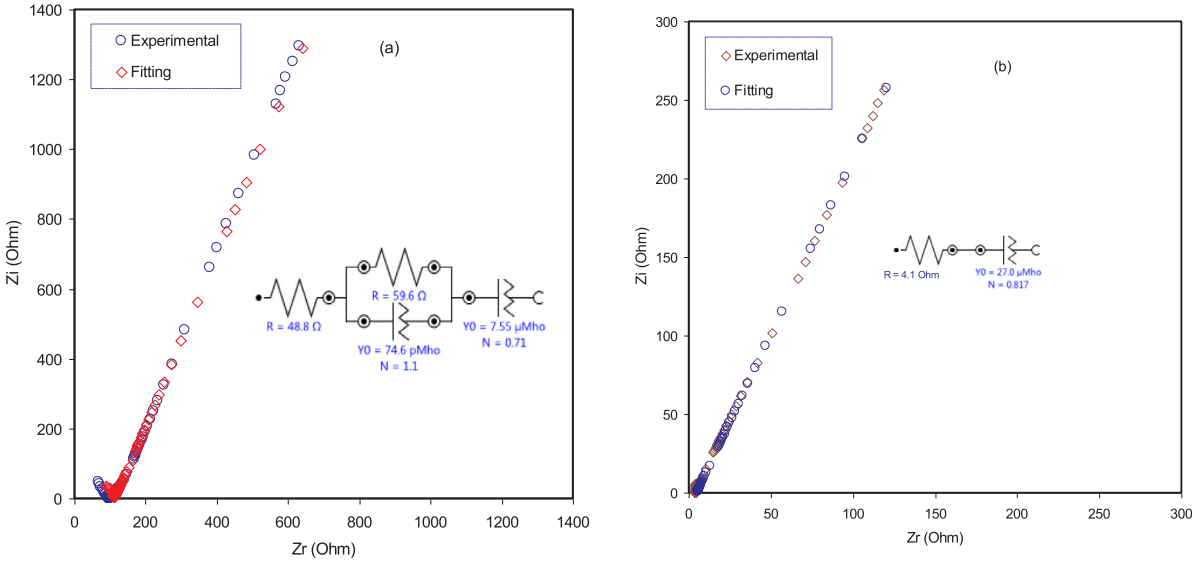

Fig. 5. Experimental Impedance and EEC fitting plots for (a) CSPB2 and (b) CSPB4 blend electrolyte films.

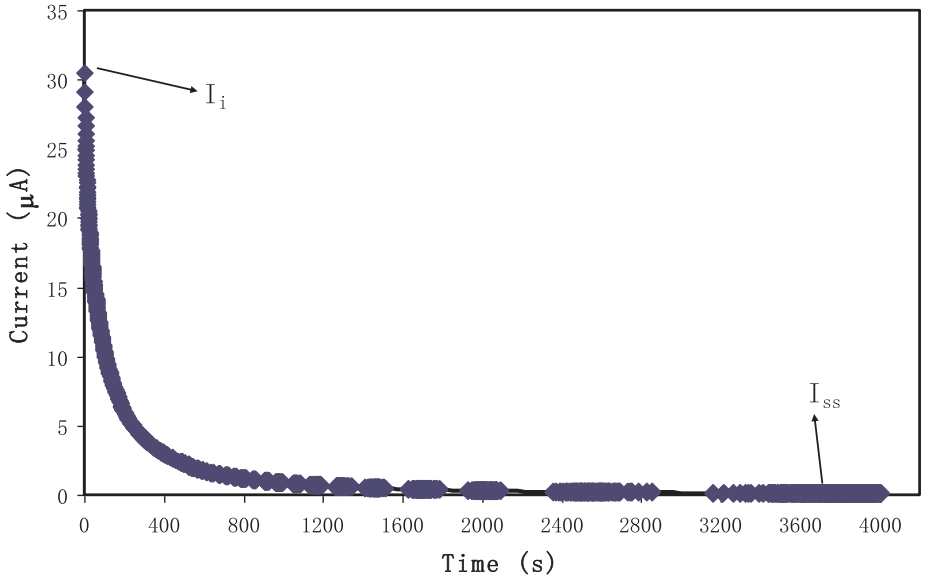

Fig. 6. Variation of current with respect to time for the cell assembled with SS/[CS:PEO]:$LiClO_4$/SS at an applied potential (ΔV) of 30 mV at ambient temperature.

be responsible for the diminishment of these electrochemical properties. In the case of the mobile ions, their preferences are to be aggregated or paired up following the rapid charge and discharge processes. Notably, it is probable for the ion pairs to block the ion transportation of the polymer electrolyte, thus impacting the rate at which ions are adsorbed at the carbon pores. In turn, this lowers the development of ion adsorption at the electrodes-electrolyte interfaces. In view of this, the energy and power density of the EDLC cells, and their specific capacitance, are linked in an inversely proportional way to the number of cycles [81]. Other researchers reported for example $4\,F\,g^{-1}$, $4.3\,F\,g^{-1}$, $8.4\,F\ g^{-1}$ and $6.5–15\,F\ g^{-1}$ for PEO9/$LiCF_3SO_3$ plasticized with 50 wt% PEG200 (PEO–NAPP)11/$LiClO_4$, PVDF–HFD (25%) + PC10–EC10/$LiClO_4$ Nafion 1100 ionomer swelled membranes, Polyurethane8/$LiClO_4$ and PVA– cellulose e–H_3PO_4 based electrolytes, respectively [82]. Thus, the outcome of C_{spe} is close to those reported in literature for polymer based electrolytes doped with Li^+ ion salts.

The equivalent series resistance (R_{esr}) is another crucial parameter need to be identified to study the internal resistance of the EDLC. R_{esr} of the EDLC can be expressed as:

$$R_{esr} = \frac{V_d}{i} \tag{10}$$

As seen in Fig. 9, there is a tiny voltage drop (V_d) prior each of the process of discharging. The voltage drop is gained in the range between 0.32 and 0.36 V which is because of the EDLC's internal resistance. Fig. 11 indicates the R_{esr} values of the EDLC for 100 cycles. The R_{esr} values of the EDLC ranges from 320 to 360 Ω. Electrolyte resistance, current collectors and the gap between current collector and electrolyte are the causes for internal resistance existence [83]. Low values of R_{esr} reveal efficient contact between electrodes and electrolytes, evidencing the facility with which ion transportation towards the surface of the electrolyte can take place, therefore developing an electrical double-layer [84]. The EDLC's ESR for this research is not high when considered in relation to the value associated with ionic liquid incorporated PEO-based polymer electrolyte (i.e., 1300 Ω) [73].

The energy density (E_d) of the fabricated EDLC can be calculated via

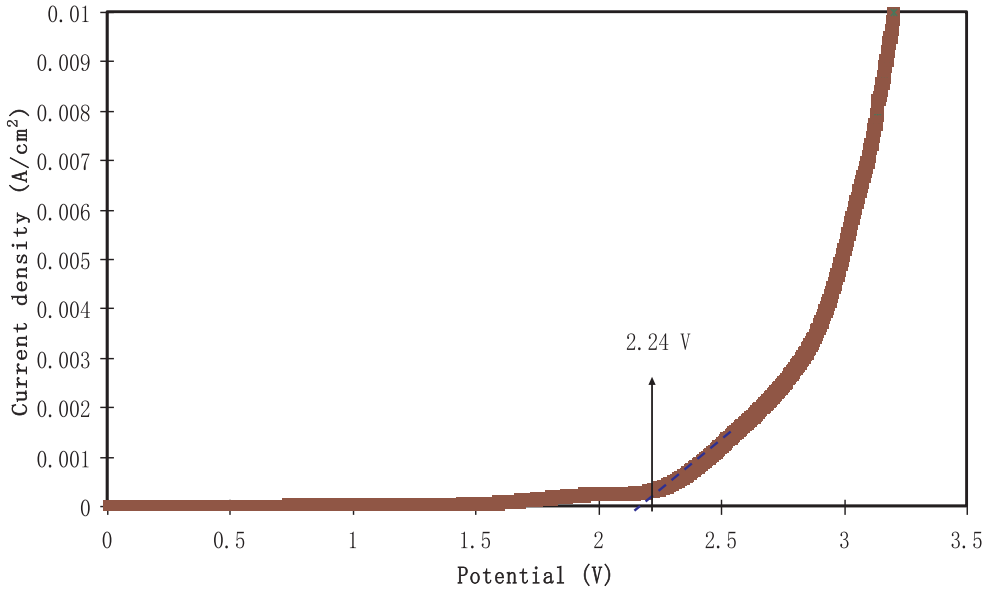

Fig. 7. LSV curve for the cell with SS/[CS:PEO]:$LiClO_4$/SS at scan rate of $50\,mV\,s^{-1}$ at ambient temperature.

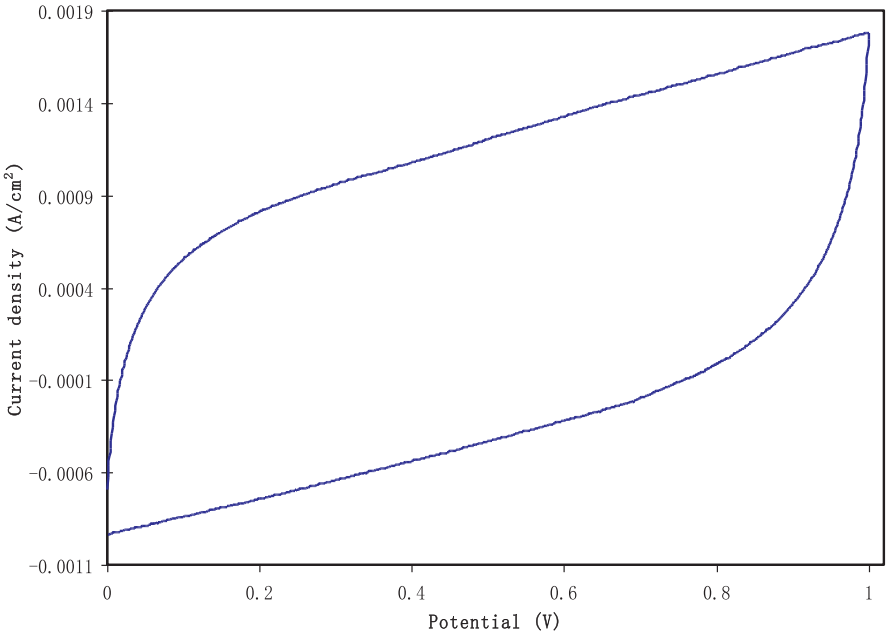

Fig. 8. CV plot of the assembled EDLC at 10 mV s^{-1} from 0 to 1 V.

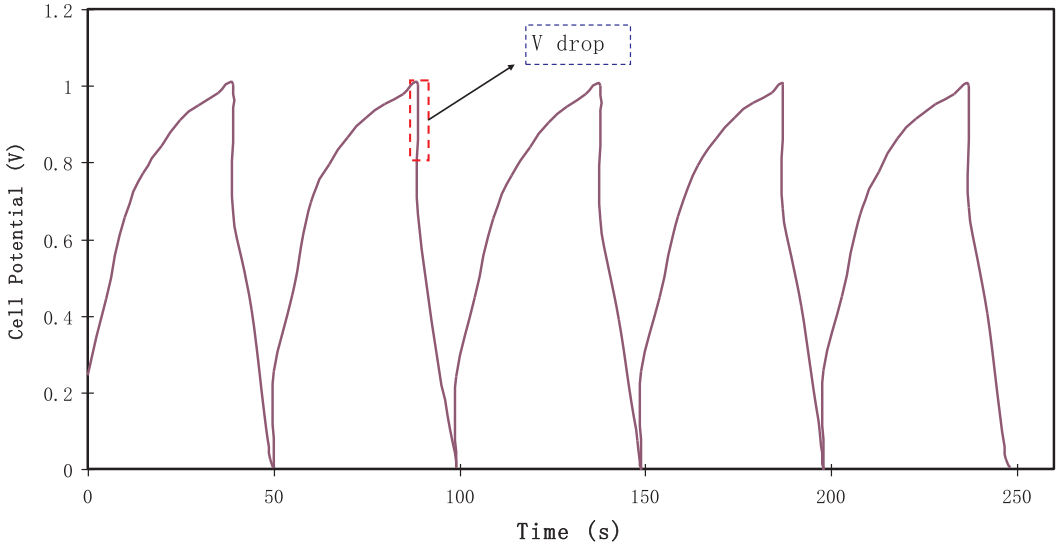

Fig. 9. Galvanostatic charge–discharge performances of the EDLC cell over first 5 cycles.

the equation:

$$E_d = \frac{C_s V}{2} \tag{11}$$

Here $V = 1$ V. Fig. 12 illustrates that E_d at the 1st cycle is 1.07 Wh kg^{-1}. The E_d is then decreases to 1.04 Wh kg^{-1} and stabilized at average of 0.94 Wh kg^{-1} from 10th cycle to 100th cycle. Hence, it can be assumed that from 10th cycle to 100th cycle, the transportation of ion possesses almost the same energy barrier [85]. The energy density achieved for the EDLC cell in the present work is of great interest compared to that reported (0.3 Wh kg^{-1}) for ionic liquid incorporated PEO based polymer electrolyte [73]. The energy density of the present work (0.94 Wh/kg) is small compared to the values (1.4 Wh/kg and 8.63 Wh kg^{-1}) reported in our previous works [86,87], while it is higher to that reported (0.86 Wh·kg^{-1}) for Chitosan:Dextran incorporated with $LiClO_4$ salt [88]. Fig. 13 portrays the power density (P_d) of the fabricated EDLC which is calculated from the equation:

$$P_d = \frac{V^2}{4mR_{esr}} \tag{12}$$

P_d of the EDLC at the 1st cycle was 321 W kg^{-1} and decreased to 311 W kg^{-1} at 5th cycle. The P_d values are detected to be in the range between 302 and 321 W kg^{-1} from 10th to 100th cycle with average of 305 W kg^{-1}. As seen in Fig. 13, the R_{esr} of the EDLC is nearly alike pattern with power density. At initial cycles the R_{esr} values are observed to raise and constant beyond 10th cycle where the P_d values reduce and gained stabilization after 10th cycle.

Conclusions

Chitosan (CS):poly (ethylene oxide) (PEO):$LiClO_4$ polymer blend electrolytes have been prepared and found to be possible for EDLC fabrication. The XRD analysis revealed that the crystalline peaks of CS decreased in CS:PEO host blend polymer due to the disruption of

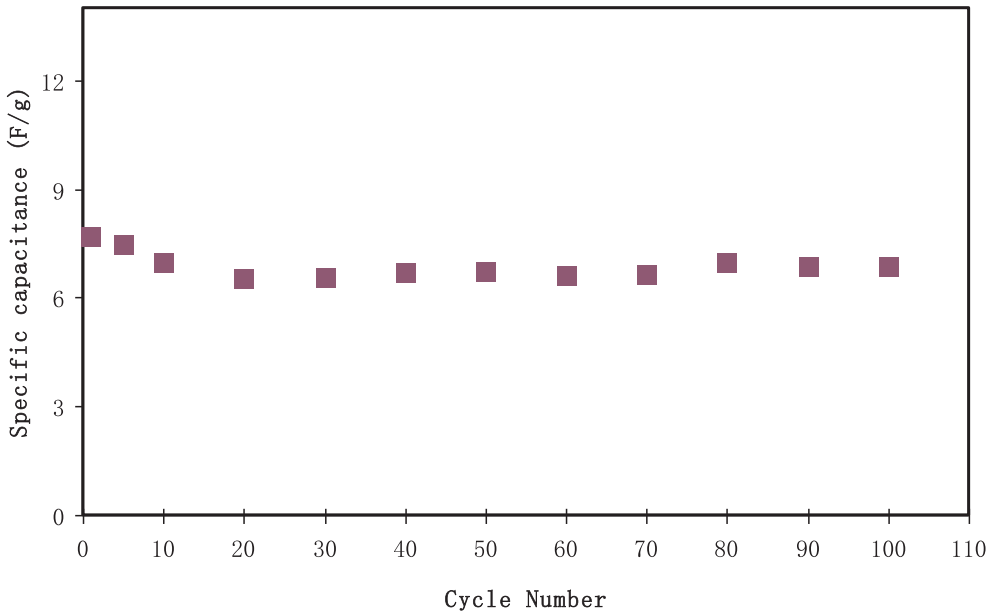

Fig. 10. Specific capacitance (C_{spe}) of the assembled EDLC up to 100th cycle.

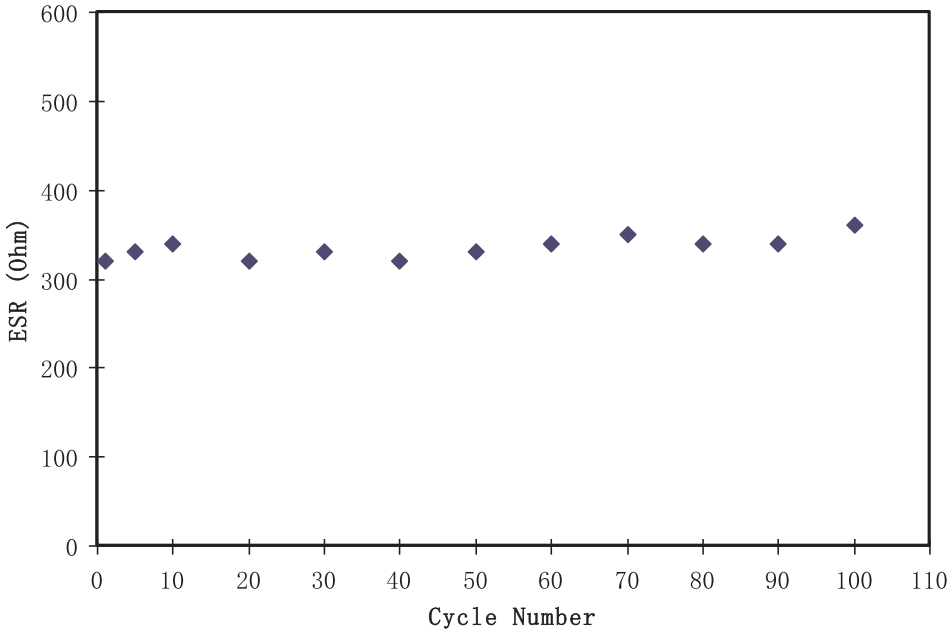

Fig. 11. Equivalent series resistance (R_{esr}) of the assembled EDLC up to 100th cycle.

molecular hydrogen bonds. The hump intensity observed in the CS:PEO polymer blend electrolyte and reduced upon addition of $LiClO_4$ salt. The FTIR analysis demonstrated the existence of complex development between the CS:PEO and incorporated salt through the shifting and lessening in the FTIR bands intensity corresponding to functional groups. The bulk resistance calculated from the impedance plots dropped with increasing the concentration of the salt. The highest DC conductivity was measured to be 7.34×10^{-4} for CS:PEO doped with 40 wt% of $LiCLO_4$ salt. With the high value of t_{ion} (0.993), ions have been considered to be the main contributor in the ionic conduction process in the polymer electrolytes. CS:PEO:$LiClO_4$ system has been observed to be stable up to 2.24 V from LSV analysis. This threshold voltage makes possible this system to be used in electrochemical devices. There were no anodic and cathodic peaks emerged in the CV plot of the EDLC which indicates the redox reaction absence at the activated carbon electrodes surface. The average C_{spe} and P_d of the assembled EDLC were 6.88F g^{-1} and 305 W kg^{-1}, respectively. The R_{esr} values were in the range between 320 and 360 Ω where E_d stabilized at 0.94 Wh kg^{-1}.

Acknowledgement

The authors gratefully acknowledge the financial support for this study from Ministry of Higher Education and Scientific Research-Kurdish National Research Council (KNRC), Kurdistan Regional Government/Iraq. The financial support from the University of Sulaimani and Komar Research Center (KRC), Komar University of Science and Technology are greatly appreciated.

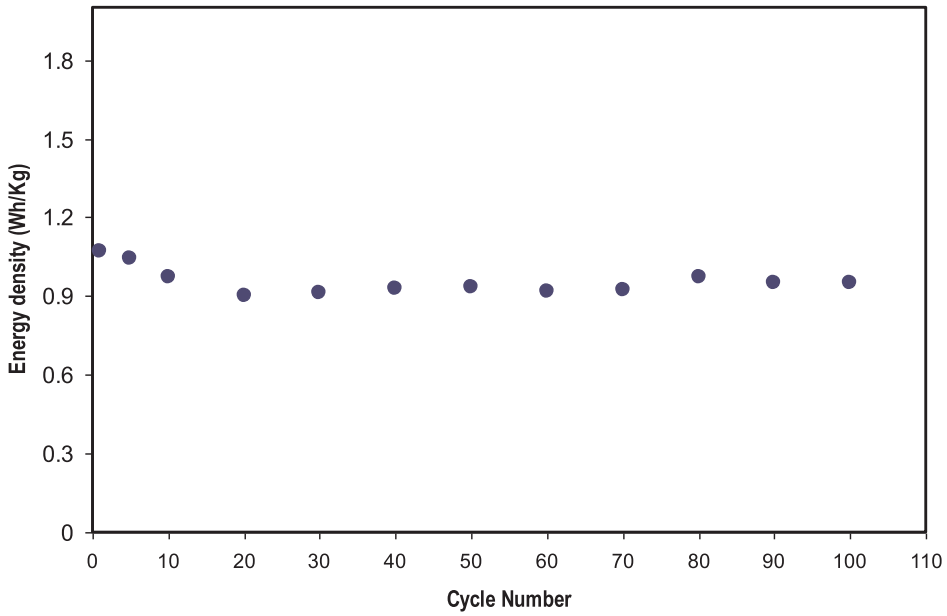

Fig. 12. Energy density (E_d) of the assembled EDLC up to 100th cycle.

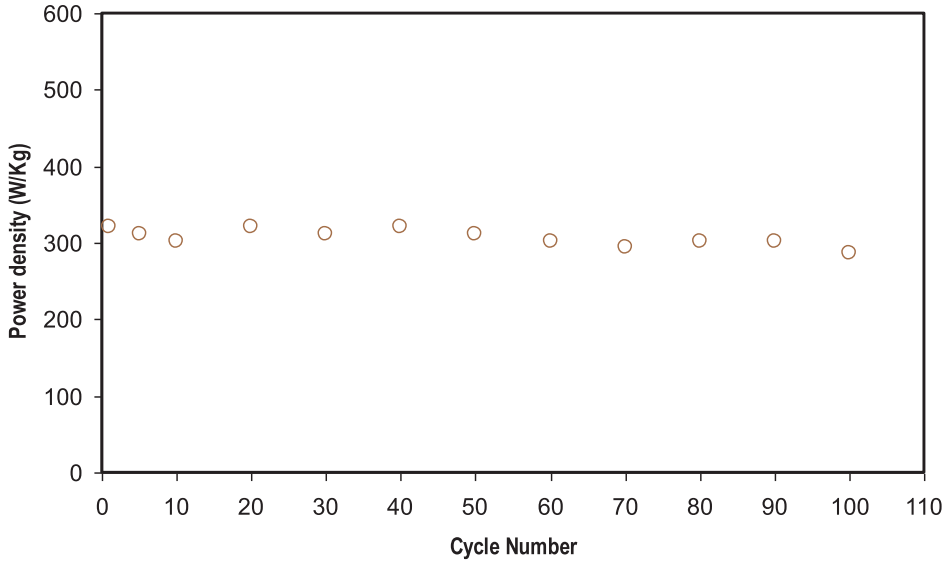

Fig. 13. Power density (P_d) of the assembled EDLC up to 100th cycle.

References

[1] Bhide A, Hariharan K. Ionic transport studies on (PEO)6:NaPO3 polymer electrolyte plasticized with PEG400. Eur Polym J 2007;43:4253–70. https://doi.org/10.1016/j.eurpolymj.2007.07.038.

[2] Li W, Yuan M, Yang M. Dual-phase polymer electrolyte with enhanced phase compatibility based on Poly (MMA-g-PVC)/PMMA. Eur Polym J 2006;42:1396–402. https://doi.org/10.1016/j.eurpolymj.2005.12.015.

[3] Ndeugueu L, Aniya M. Structural characterization of the ac conductivity in Ag ion conducting glasses. J Mater Sci 2009;44:2483–8. https://doi.org/10.1007/s10853-009-3318-x.

[4] Matabola KP, De Vries AR, Moolman FS, Luyt AS. Single polymer composites: a review. J Mater Sci 2009;44:6213–22. https://doi.org/10.1007/s10853-009-3792-1.

[5] Stephan AM. Review on gel polymer electrolytes for lithium batteries. Eur Polym J 2006;42:21–42. https://doi.org/10.1016/j.eurpolymj.2005.09.017.

[6] Zhou S, Fang S. High ionic conductivity of all-solid polymer electrolytes based on polyorganophosphazenes. Eur Polym J 2007;43:3695–700. https://doi.org/10.1016/j.eurpolymj.2007.06.001.

[7] Kim JH, Won J, Kang YS. Olefin-induced dissolution of silver salts physically dispersed in inert polymers and their application to olefin/paraffin separation. J Memb Sci 2004;241:403–7. https://doi.org/10.1016/j.memsci.2004.05.027.

[8] Salleh NS, Aziz SB, Aspanut Z, Kadir MFZ. Electrical impedance and conduction mechanism analysis of biopolymer electrolytes based on methyl cellulose doped with ammonium iodide. Ionics (Kiel) 2016;22:2157–67. https://doi.org/10.1007/s11581-016-1731-0.

[9] Senthil RA, Theerthagiri J, Madhavan J, Arof AK. Enhanced performance of dye-sensitized solar cell using 2-mercaptobenzothiazole-doped poly(vinylidinefluoride-co-hexafluoropropylene) polymer electrolyte. Ionics (Kiel) 2016;22:1225–30. https://doi.org/10.1007/s11581-016-1642-0.

[10] Theerthagiri J, Madhavan J. Organic dopant added polyvinylidene fluoride based solid polymer electrolytes for dye-sensitized solar cells. J Phys Chem Solids 2016;89:78–83. https://doi.org/10.1016/j.jpcs.2015.11.003.

[11] Senthil RA, Theerthagiri J, Madhavan J, Arof AK. Performance characteristics of guanine incorporated PVDF-HFP/PEO polymer blend electrolytes with binary iodide salts for dye-sensitized solar cells. Opt Mater (Amst) 2016;58:357–64. https://doi.org/10.1016/j.optmat.2016.06.007.

[12] Senthil RA, Theerthagiri J, Madhavan J, Murugan K, Arunachalam P, Arof AK. Enhanced performance of dye-sensitized solar cells based on organic dopant incorporated PVDF-HFP/PEO polymer blend electrolyte with g-C_3N_4/TiO_2 photoanode. J Solid State Chem 2016;242:199–206. https://doi.org/10.1016/j.jssc.2016.07.020.

[13] Senthil RA, Theerthagiri J, Madhavan J, Arof AK. Dye-sensitized solar cell using 4-chloro-7-nitrobenzofurazan incorporated polyvinyl alcohol polymer electrolyte. Indian J Phys 2016;90:1265–70. https://doi.org/10.1007/s12648-016-0869-y.

[14] Hamsan MH, Shukur MF, Aziz SB, Kadir MFZ. Dextran from Leuconostoc mesenteroides-doped ammonium salt-based green polymer electrolyte. Bull Mater Sci 2019;3:57. https://doi.org/10.1007/s12034-019-1740-5.

[15] Hirase R, Higashiyama Y, Mori M, Takahara Y, Yamane C. Hydrated salts as both solvent and plasticizer for chitosan. Carbohydr Polym 2010;80:993–6. https://doi.org/10.1016/j.carbpol.2010.01.001.

[16] Si Trung T, Thein-han WW, Thi N, Ng C-H, Stevens W. Functional characteristics of shrimp chitosan and its membranes as affected by the degree of deacetylation. Bioresour Technol 2006;97:659–63. https://doi.org/10.1016/j.biortech.2005.03.023.

[17] Bai P, Cao F, Lan X, Zhao F, Ma Y, Zhao C. Chitosan gel beads immobilized Cu (II) for selective adsorption of amino acids. J Biochem Biophys Methods 2008;70:903–8. https://doi.org/10.1016/j.jprot.2008.01.001.

[18] Lu G, Kong L, Sheng B, Wang G, Gong Y, Zhang X. Degradation of covalently cross-linked carboxymethyl chitosan and its potential application for peripheral nerve regeneration. Eur Polym J 2007;43:3807–18. https://doi.org/10.1016/j.eurpolymj.2007.06.016.

[19] Ng LS, Mohamad AA. Protonic battery based on a plasticized chitosan-NH_4 NO_3 solid polymer electrolyte. J Power Sources 2006;163:382–5. https://doi.org/10.1016/j.jpowsour.2006.09.042.

[20] Khiar ASA, Puteh R, Arof AK. Conductivity studies of a chitosan-based polymer electrolyte. Phys B Condens Matter 2006;373:23–7. https://doi.org/10.1016/j.physb.2005.10.104.

[21] Osman Z, Ibrahim ZA, Arof AK. Conductivity enhancement due to ion dissociation in plasticized chitosan based polymer electrolytes. Carbohydr Polym 2001;44:167–73. https://doi.org/10.1016/S0144-8617(00)00236-8.

[22] Buraidah MH, Teo LP, Majid SR, Arof AK. Ionic conductivity by correlated barrier hopping in NH_4I doped chitosan solid electrolyte. Phys B Condens Matter 2009;404:1373–9. https://doi.org/10.1016/j.physb.2008.12.027.

[23] Kadir MFZ, Majid SR, Arof AK. Plasticized chitosan – PVA blend polymer electrolyte based proton battery. Electrochim Acta 2010;55:1475–82. https://doi.org/10.1016/j.electacta.2009.05.011.

[24] Subban RHY, Arof AK, Radhakrishna S. Polymer batteries with chitosan electrolyte mixed with sodium perchlorate. Mater Sci Eng, B 1996;38:156–60. https://doi.org/10.1016/0921-5107(95)01508-6.

[25] Morni NM, Mohamed NS, Arof AK. Silver nitrate doped chitosan acetate films and electrochemical cell performance. Mater Sci Eng, B 1997;45:140–6. https://doi.org/10.1016/S0921-5107(96)02023-5.

[26] El-sawy NM, Abd El-rehim HA, Elbarbary AM, Hegazy EA. Radiation-induced degradation of chitosan for possible use as a growth promoter in agricultural purposes. Carbohydr Polym 2010;79:555–62. https://doi.org/10.1016/j.carbpol.2009.09.002.

[27] Nagahama H, Maeda H, Kashiki T, Jayakumar R, Furuike T, Tamura H. Preparation and characterization of novel chitosan/gelatin membranes using chitosan hydrogel. Carbohydr Polym 2009;76:255–60. https://doi.org/10.1016/j.carbpol.2008.10.015.

[28] Koduru HK, Iliev MT, Kondamareddy KK, Karashanova D, Vlakhov T, Zhao X-Z, et al. Investigations on Poly (ethylene oxide) (PEO) - blend based solid polymer electrolytes for sodium ion batteries. J Phys Conf Ser 2016;764:1–8. https://doi.org/10.1088/1742-6596/764/1/012006.

[29] Yang Y, Inoue T, Fujinami T, Mehta MA. Ionic conductivity and interfacial properties of polymer electrolytes based on PEO and boroxine ring polymer. J Appl Polym Sci 2002;84:17–21. https://doi.org/10.1002/app.10090.

[30] Chun-guey W, Chiung-hui W, Ming-i L, Huey-jan C. New solid polymer electrolytes based on PEO/PAN hybrids. J Appl Polym Sci 2005;99:1530–40. https://doi.org/10.1002/app.22250.

[31] Kim M, Lee L, Jung Y, Kim S. Study on Ion conductivity and crystallinity of composite polymer electrolytes based on poly (ethylene oxide)/poly (acrylonitrile) containing nano-sized Al_2O_3 fillers. J Nanosci Nanotechnol 2013;13:7865–9. https://doi.org/10.1166/jnn.2013.8107.

[32] Jo G, Jeon H, Park MJ. Synthesis of polymer electrolytes based on poly(ethylene oxide) and an anion-stabilizing hard polymer for enhancing conductivity and cation transport. ACS Macro Lett 2015;4:225–30. https://doi.org/10.1021/mz500717j.

[33] Aziz SB, Abdullah RM. Crystalline and amorphous phase identification from the tanδ relaxation peaks and impedance plots in polymer blend electrolytes based on [CS:AgNt]x:PEO(x–1)($10 \leq x \leq 50$). Electrochim Acta 2018;285:30–46. https://doi.org/10.1016/j.electacta.2018.07.233.

[34] Iro ZS, Subramani C, Dash SS. A brief review on electrode materials for supercapacitor. Int J Electrochem Sci 2016;11:10628–43. https://doi.org/10.20964/2016.12.50.

[35] Inagaki M, Konno H, Tanaike O. Carbon materials for electrochemical capacitors. J Power Sources 2010;195:7880–903. https://doi.org/10.1016/j.jpowsour.2010.06.036.

[36] Zhang D, Zhang X, Chen Y, Yu P, Wang C, Ma Y. Enhanced capacitance and rate capability of graphene/polypyrrole composite as electrode material for supercapacitors. J Power Sources 2011;196:5990–6. https://doi.org/10.1016/j.jpowsour.2011.02.090.

[37] Pell WG, Conway BE. Peculiarities and requirements of asymmetric capacitor devices based on combination of capacitor and battery-type electrodes. J Power Sources 2004;136:334–45. https://doi.org/10.1016/j.jpowsour.2004.03.021.

[38] Shukur MF, Ithnin R, Kadir MFZ. Protonic transport analysis of starch-chitosan blend based electrolytes and application in electrochemical device. Mol Cryst Liq Cryst 2014;603:52–65. https://doi.org/10.1080/15421406.2014.966259.

[39] Göktepe F, Çelik SÜ, Bozkurt A. Preparation and the proton conductivity of chitosan/poly (vinyl phosphonic acid) complex polymer electrolytes. J Non Cryst Solids 2008;354:3637–42. https://doi.org/10.1016/j.jnoncrysol.2008.03.023.

[40] Aziz SB, Abidin ZHZ, Kadir MFZ. Innovative method to avoid the reduction of silver ions to silver nanoparticles ($Ag+ \rightarrow Ago$) in silver ion conducting based polymer electrolytes. Phys Scr 2015;90:35808. https://doi.org/10.1088/0031-8949/90/3/035808.

[41] Wan Y, Creber KAM, Peppley B, Bui VT. Chitosan-based solid electrolyte composite membranes: I. Preparation and characterization. J Membr Sci 2006;280:666–74. https://doi.org/10.1016/j.memsci.2006.02.024.

[42] Aziz SB. Role of dielectric constant on ion transport : reformulated Arrhenius equation. Adv Mater Sci Eng 2016;2016:11. https://doi.org/10.1155/2016/2527013.

[43] Smitha B, Sridhar S, Khan AA. Chitosan – sodium alginate polyion complexes as fuel cell membranes. Eur Polym J 2005;41:1859–66. https://doi.org/10.1016/j.eurpolymj.2005.02.018.

[44] Aziz SB, Abidin ZHZ, Arof AK. Effect of silver nanoparticles on the DC conductivity in chitosan – silver triflate polymer electrolyte. Phys B Phys Condens Matter 2010;405:4429–33. https://doi.org/10.1016/j.physb.2010.08.008.

[45] Hashmi SA, Chandra S. Experimental investigations on a sodium-ion-conducting polymer electrolyte based on poly (ethylene oxide) complexed with $NaPF_6$. Mater Sci Eng, B 1995;34:18–26. https://doi.org/10.1016/0921-5107(95)01219-2.

[46] Sanders RA, Snow AG, Frech R, Glatzhofer DT. A spectroscopic and conductivity comparison study of linear poly (N -methylethylenimine) with lithium triflate and sodium triflate. Electrochim Acta 2003;48:2247–53. https://doi.org/10.1016/S0013-4686(03)00211-1.

[47] Dumitraşcu M, Meltzer V, Sima E, Vîrgolic M, Albu MG, Ficai A, et al. Characterization of electron beam irradiated collagen-polyvinylpyrrolidone (pvp) and collagen-dextran (dex) blends. Dig J Nanomater Biostructures 2011;6:1793–803.

[48] Agrawal P, Strijkers GJ, Nicolay K. Chitosan-based systems for molecular imaging. Adv Drug Deliv Rev 2010;62:42–58. https://doi.org/10.1016/j.addr.2009.09.007.

[49] Aziz SB, Abidin ZHZ. Electrical conduction mechanism in solid polymer electrolytes: new concepts to Arrhenius equation. J Soft Matter 2013;2013:1–8. https://doi.org/10.1155/2013/323868.

[50] Aziz SB, Marif RB, Brza MA, Hassan AN, Ahmad HA, Faidhalla YA, et al. Structural, thermal, morphological and optical properties of PEO filled with biosynthesized Ag nanoparticles: new insights to band gap study. Results Phys 2019;13:102220https://doi.org/10.1016/j.rinp.2019.102220.

[51] Buraidah MH, Arof AK. Characterization of chitosan/PVA blended electrolyte doped with NH4I. J Non Cryst Solids 2011;357:3261–6. https://doi.org/10.1016/j.jnoncrysol.2011.05.021.

[52] Kadir MFZ, Aspanut Z, Majid SR, Arof AK. FTIR studies of plasticized poly (vinyl alcohol)– chitosan blend doped with NH_4NO_3 polymer electrolyte membrane. Spectrochim Acta Part A Mol Biomol Spectrosc 2011;78:1068–74. https://doi.org/10.1016/j.saa.2010.12.051.

[53] Wei D, Sun W, Qian W, Ye Y, Ma X. The synthesis of chitosan-based silver nanoparticles and their antibacterial activity. Carbohydr Res 2009;344:2375–82. https://doi.org/10.1016/j.carres.2009.09.001.

[54] Suvarna RP, Rao KR, Subbarangaiah K. A simple technique for a.c. conductivity measurements. Bull Mater Sci 2002;25:647–51. https://doi.org/10.1007/BF02707898.

[55] Venkateswarlu M, Satyanarayana N. AC conductivity studies of silver based fast ion conducting glassy materials for solid state batteries. Mater Sci Eng, B 1998;54:189–95. https://doi.org/10.1016/S0921-5107(98)00156-1.

[56] Jacob MME, Prabaharan SRS, Radhakrishna S. Effect of PEO addition on the electrolytic and thermal properties of PVDF-$LiClO_4$ polymer electrolytes. Solid State Ionics 1997;104:267–76. https://doi.org/10.1016/S0167-2738(97)00422-0.

[57] Fonseca Jr CP, Cavalcante F, Amaral FA, Souza CAZ, Neves S. Thermal and conduction properties of a PCL-biodegradable gel polymer electrolyte with $LiClO_4$, LiF_3CSO_3, and $LiBF_4$ salts. Int J Electrochem Sci 2007;2:52–63.

[58] Pradhan DK, Choudhary P, Samantaray BK, Karan NK, Katiyar RS. Effect of plasticizer on structural and electrical properties of polymer nanocompsoite electrolytes. Int J Electrochem Sci 2007;2:861–71.

[59] Mohapatra SR, Thakur AK, Choudhary RNP. Effect of nanoscopic confinement on improvement in ion conduction and stability properties of an intercalated polymer nanocomposite electrolyte for energy storage applications. J Power Sources 2009;191:601–13. https://doi.org/10.1016/j.jpowsour.2009.01.100.

[60] Aziz SB, Abdullah RM, Kadir MFZ, Ahmed HM. Non suitability of silver ion conducting polymer electrolytes based on chitosan mediated by barium titanate ($BaTiO_3$) for electrochemical device applications. Electrochim Acta 2019;296:494–507. https://doi.org/10.1016/j.electacta.2018.11.081.

[61] Shukur MF, Ithnin R, Kadir MFZ. Electrical characterization of corn starch-LiOAc electrolytes and application in electrochemical double layer capacitor. Electrochim Acta 2014;136:204–16. https://doi.org/10.1016/j.electacta.2014.05.075.

[62] Teo LP, Buraidah MH, Nor AFM, Majid SR. Conductivity and dielectric studies of Li_2SnO_3. Ionics (Kiel) 2012;18:655–65. https://doi.org/10.1007/s11581-012-0667-2.

[63] Rajendran S, Sivakumar P. Investigations on PVC/PAN composite polymer electrolytes. J Memb Sci 2008;315:67–73. https://doi.org/10.1016/j.memsci.2008.02.007.

[64] Aziz SB, Kadir MFZ, Abidin ZHZ. Structural, morphological and electrochemical impedance study of CS:LiTf based solid polymer electrolyte: reformulated Arrhenius equation for ion transport study. Int J Electrochem Sci 2016;11:9228–44. https://doi.org/10.20964/2016.11.18.

[65] Aziz SB, Karim WO, Qadir KW, Zafar Q. Proton Ion conducting solid polymer electrolytes based on chitosan incorporated with various amounts of barium titanate ($BaTiO_3$). Int J Electrochem Sci 2018;13:6112–25. https://doi.org/10.20964/2018.06.38.

[66] Tripathi M, Tripathi SK. Electrical studies on ionic liquid-based gel polymer electrolyte for its application in EDLCs. Ionics (Kiel) 2017;23:2735–46. https://doi.org/10.1007/s11581-017-2051-8.
[67] Kufian MZ, Aziz MF, Shukur MF, Rahim AS, Ariffin NE, Shuhaimi NEA, et al. PMMA – LiBOB gel electrolyte for application in lithium ion batteries. Solid State Ionics 2012;208:36–42. https://doi.org/10.1016/j.ssi.2011.11.032.
[68] Diederichsen KM, Mcshane EJ, Mccloskey BD. Promising routes to a High Li^+ transference number electrolyte for lithium ion batteries. ACS Energy Lett 2017;2:2563–75. https://doi.org/10.1021/acsenergylett.7b00792.
[69] Amudha S, Suthanthiraraj SA. Silver ion conducting characteristics of a polyethylene oxide-based composite polymer electrolyte and application in solid state batteries. Adv Mater Lett 2015;6:874–82. https://doi.org/10.5185/amlett.2015.5831.
[70] Pande GP, Kumar Y, Hashmi SA. Ionic liquid incorporated polymer electrolytes for supercapacitor application. Indian J Chem 2010;49A:743–51http://hdl.handle.net/123456789/9673.
[71] Sampathkumar L, Selvin PC, Selvasekarapandian S, Perumal P, Chitra R, Muthukrishnan M. Synthesis and characterization of biopolymer electrolyte based on tamarind seed polysaccharide, lithium perchlorate and ethylene carbonate for electrochemical applications. Ionics (Kiel) 2019;25:1067–82. https://doi.org/10.1007/s11581-019-02857-1.
[72] Monisha S, Mathavan T, Selvasekarapandian S, Benial AM, Latha MP. Preparation and characterization of cellulose acetate and lithium nitrate for advanced electrochemical devices. Ionics (Kiel) 2016;23:2697–706. https://doi.org/10.1007/s11581-016-1886-8.
[73] Pandey GP, Kumar Y, Hashmi SA. Ionic liquid incorporated PEO based polymer electrolyte for electrical double layer capacitors: a comparative study with lithium and magnesium systems. Solid State Ionics 2011;190:93–8. https://doi.org/10.1016/j.ssi.2011.03.018.
[74] Winie T, Jamal A, Saaid FI, Tseng T. Hexanoyl chitosan/ENR25 blend polymer electrolyte system for electrical double layer capacitor. Polym Adv Technol 2018;30:726–35. https://doi.org/10.1002/pat.4510.
[75] Woo HJ, Liew C, Majid SR, Arof AK. Poly (ε-caprolactone)-based polymer electrolyte for electrical double-layer capacitors. High Perform Polym 2014;26:637–40. https://doi.org/10.1177/0954008314542168.
[76] Kadir MFZ, Arof AK. Application of PVA – chitosan blend polymer electrolyte membrane in electrical double layer capacitor. Mater Res Innov 2011;15:s217–20. https://doi.org/10.1179/143307511X13031890749299.
[77] Prabaharan SRS, Vimala R, Zainal Z. Nanostructured mesoporous carbon as electrodes for supercapacitors. J Power Sources 2006;161:730–6. https://doi.org/10.1016/j.jpowsour.2006.03.074.
[78] Kumar Y, Pandey GP, Hashmi SA. Gel polymer electrolyte based electrical double layer capacitors: comparative study with multiwalled carbon nanotubes and activated carbon electrodes. J Phys Chem C 2012;116:26118–27. https://doi.org/10.1021/jp305128z.
[79] Fattah NFA, Ng HM, Mahipal YK, Numan A, Ramesh S, Ramesh K. An approach to solid-state electrical double layer capacitors fabricated with graphene oxide-doped Ionic Liquid-Based Solid Copolymer Electrolytes. Materials (Basel) 2016;9:450. https://doi.org/10.3390/ma9060450.
[80] Das S, Ghosh A. Solid polymer electrolyte based on PVDF-HFP and ionic liquid embedded with TiO2 nanoparticle for electric double layer capacitor (EDLC) application. J Electrochem Soc 2017;164:1348–53. https://doi.org/10.1149/2.0561713jes.
[81] Liew C, Ramesh S, Arof AK. Enhanced capacitance of EDLCs (electrical double layer capacitors) based on ionic liquid-added polymer electrolytes. Energy 2016;109:546–56. https://doi.org/10.1016/j.energy.2016.05.019.
[82] Shuhaimi NEA, Alias NA, Majid SR, Arof AK. Electrical double layer capacitor with proton conducting K -carrageenan – chitosan electrolytes. Funct Mater Lett 2008;1:195–201. https://doi.org/10.1142/S1793604708000423.
[83] Arof AK, Kufian MZ, Syukur MF, Aziz MF, Abdelrahman AE, Majid SR. Electrical double layer capacitor using poly (methyl methacrylate)–C4BO8Li gel polymer electrolyte and carbonaceous material from shells of mata kucing (Dimocarpus longan) fruit. Electrochim Acta 2012;74:39–45. https://doi.org/10.1016/j.electacta.2012.03.171.
[84] Asmara SN, Kufian MZ, Majid SR, Arof AK. Preparation and characterization of magnesium ion gel polymer electrolytes for application in electrical double layer capacitors. Electrochim Acta 2011;57:91–7. https://doi.org/10.1016/j.electacta.2011.06.045.
[85] Shukur MF. Characterization of ion conducting solid biopolymer electrolytes based on starch-chitosan blend and application in electrochemical devices Dissertation Malaysia: University of Malaya; 2015.
[86] Aziz SB, Hamsan MH, Karim WO, Kadir MFZ, Brza MA, Abdullah OGh. High proton conducting polymer blend electrolytes based on chitosan: dextran with constant specific capacitance and energy density. Biomolecules 2019;9(7):267. https://doi.org/10.3390/biom9070267.
[87] Hamsan MH, Abdullah RM, Kadir MFZ. A Promising polymer blend electrolytes based on chitosan: methyl cellulose for EDLC application with high specific capacitance and energy density. Molecules 2019;24(13):2503. https://doi.org/10.3390/molecules24132503.
[88] Shujahadeen BA, Hamsan Muhamad H. Development of polymer blend electrolyte membranes based on chitosan: dextran with high ion transport properties for EDLC application. Int J Mol Sci 2019;20(13):3369. https://doi.org/10.3390/ijms20133369.